CHIRAL MAGNETIC EFFECT AND ELECTROMAGNETIC FIELD EVOLUTION*

V.D. Toneev, V. Voronyuk

Joint Institute for Nuclear Research, Dubna, Russia
and
Frankfurt Institute for Advanced Studies, Frankfurt, Germany

(Received January 2, 2012)

The energy dependence of the observable two-particle correlator in search for local strong parity violation in Au+Au collisions is estimated within a simple phenomenological model. The model reproduces available RHIC data but predicts that at LHC the chiral magnetic effect (CME) will be about 20 times weaker than at RHIC, contrary to the first LHC measurements. In the lower energy range, this effect should vanish sharply at an energy somewhere above the top SPS one in agreement with the preliminary results of the Beam Energy Scan program. To elucidate CME background effects a transport HSD model including magnetic field evolution is put forward and electromagnetic dynamics at RHIC energies is investigated. It is observed that the electromagnetic field included into the hadronic model does not influence on observables due to mutual compensation of effects of electric and magnetic fields.

DOI:10.5506/APhysPolBSupp.5.887
PACS numbers: 25.75.–q, 25.75.Ag

1. Introduction

The existence of nontrivial topological configurations in QCD vacuum is a fundamental property of the gauge theory though until now there is no direct experimental evidence for topological effects. Transitions between different topological states occur with the change of the topological number $n_{\rm w}$ characterizing these states and induce anomalous processes like local violation of the $\mathcal{P}$ and $\mathcal{CP}$ symmetry. The interplay of these topological configurations with (chiral) quarks results in the local imbalance of chirality. Such chiral asymmetry coupled to a strong magnetic field, created by colliding nuclei perpendicularly to the reaction plane, induces a current of

* Talk presented at HIC for FAIR Workshop and XXVIII Max Born Symposium "Three Days on Quarkyonic Island", Wrocław, Poland, May 19–21, 2011.

electric charge along the direction of a magnetic field which leads to a separation of oppositely charged particles with respect to the reaction plane. Thus, as was argued in Refs. [1,2,3,4,5] the topological effects in QCD may be observed in heavy ion collisions directly in the presence of very intense external magnetic fields due to the "Chiral Magnetic Effect" (CME) as a manifestation of spontaneous violation of the $\mathcal{CP}$ symmetry. It was shown that the electromagnetic field of the required strength can be created in relativistic heavy-ion collisions [3, 6]. First experimental evidence for the CME identified via the observed charge separation effect with respect to the reaction plane was presented by the STAR Collaboration at RHIC [7]. Recently preliminary data below the nominal RHIC energy (Beam Energy Scan program) [8] and at the LHC energy [9] have been obtained.

In this paper, we shortly remain our analysis of the first STAR data [10] and compare results with a new finding. In respect to the CME, we also make a dynamical estimate of the CME background based on the nonequalibrium Hadron-String-Dynamics (HSD) microscopical transport approach [11] supplemented by the treatment of electromagnetic field evolution.

2. CME in a simple model

We remind here our phenomenological model used in the CME analysis in Ref. [10].

For one-dimensional random walk in the topological number space the topological charge (winding number) $n_{\rm w}$ generated during the time τ_B, when the magnetic field is present, may be estimated as

$$n_{\rm w} \equiv \sqrt{Q_{\rm s}^2} = \sqrt{\Gamma_{\rm S}\, V\, \tau_B} \sim \sqrt{\frac{dN_{\rm hadrons}}{dy}}\, \sqrt{Q_{\rm s}\ \tau_B}\,, \tag{1}$$

where $\Gamma_{\rm S}$ is the sphaleron transition rate which in weak and strong coupling $\Gamma_{\rm S} \sim T^4$ with different coefficients. The initial temperature T_0 of the produced matter at time $\tau \simeq 1/Q_{\rm s}$ is proportional to the saturation momentum $Q_{\rm s}$, $T_0 = c\ Q_{\rm s}$. In the last semiequality of (1), the expansion time and the corresponding time dependence of the temperature are neglected. Since sizable sphaleron transitions occur only in the deconfined phase, the time τ_B in Eq. (1) is really the smallest lifetime between the strong magnetic field $\tilde{\tau}_B$ one and the lifetime of deconfined matter τ_ϵ: $\tau_B = \min\{\tilde{\tau}_B, \tau_\epsilon\}$.

The measured electric charge particle asymmetry is associated with the averaged correlator a by the following relation [12]

$$\langle\cos(\psi_\alpha + \psi_\beta - 2\Psi_{\rm RP})\rangle = \langle\cos(\psi_\alpha + \psi_\beta - 2\Psi_c)\rangle/v_{2,c} = v_{1,\alpha}v_{1,\beta} - a_\alpha a_\beta\,, \tag{2}$$

where $\Psi_{\rm RP}$ is the azimuthal angle of the reaction plane defined by the beam axis and the line joining the centers of colliding nuclei. Averaging in (2)

is carried out over the whole event ensemble. The second equality in (2) corresponds to azimuthal measurements with respect to particle of type c extracted from three-body correlation analysis [12], v_1 and v_2 are the directed and elliptic flow parameters, respectively. According to Ref. [1], an average correlator $a = \sqrt{a_\alpha a_\beta}$ is related to the topological charge, $n_{\rm w}$, as

$$a \sim \frac{n_{\rm w}}{dN_{\rm hadrons}/dy} \sim \frac{\sqrt{Q_{\rm s}\tau_B}}{\sqrt{dN_{\rm hadrons}/dy}} \sim \sqrt{\frac{\tau_B}{Q_{\rm s}}} \sim (\sqrt{s_{NN}})^{-1/16}\sqrt{\tau_B}\,, \qquad (3)$$

where absorption and rescattering in dense matter are neglected for the same and opposite charge correlations. In the last equality we assumed that $Q_{\rm s}^2 \sim s_{NN}^{1/8} \sim dN_{\rm hadrons}/dy$ [13].

As follows from Eq. (3), the $\mathcal{CP}$ violation effect can be quantified by the correlator

$$a^2 = K_{\rm Au}\,(\sqrt{s_{NN}})^{-1/8}\,\tau_B\,. \qquad (4)$$

The normalization constant $K_{\rm Au}$ can be tuned at the reference energy $\sqrt{s_{NN}} = 200\,{\rm GeV}$ from the inverse relation (3) and experimental value $a_{\rm exp}$ at this energy for $b = 10\,{\rm fm}$

$$K_{\rm Au} = \frac{a_{\rm exp}^2\,(200)^{1/8}}{\tau_B(200)}\,. \qquad (5)$$

The only quantity needed is the lifetime τ_B defined as the time during which the magnetic field is above the critical value $B_{\rm crit}$ needed to support a fermion Landau level on the domain wall $eB_{\rm crit} = 2\pi/S_{\rm d}$, where $S_{\rm d}$ is the domain wall area. Since the size of the domain wall is not reliably known, it is hard to pin down the number, but it should be of the order of m_π^2. Thus, we have to treat $B_{\rm crit}$ as a free parameter which defines the lifetime from the calculated $B(t)$ distribution [10]. As to the impact parameter distribution, the CME is assumed to be roughly linear in b/R Ref. [3]. Taking this as a hypothesis we evaluate the centrality dependence of the CME fitting this line to points $b = 10\,{\rm fm}$ (or centrality (40–50)%) to be estimated in our model and $b = 0$, where the CME is zero. The results are presented in Fig. 1 for Au+Au collisions. As is seen, the calculated lines quite reasonably reproduce the measured points of azimuthal asymmetry of same-charge particles for Au+Au collisions at $\sqrt{s_{NN}} = 200$ and $62\,{\rm GeV}$. The chosen critical field value $eB_{\rm crit} = 0.7\ m_\pi^2$ results in absence of the CME above the top SPS energy because the critical magnetic field practically coincides with the maximal field at this bombarding energy. This finding is in a qualitative agreement with very recent preliminary STAR results that the difference between same-charge and opposite charge correlations is decreasing with decreasing beam energy what takes place at $\sqrt{s_{NN}} < 40\,{\rm GeV}$ [8].

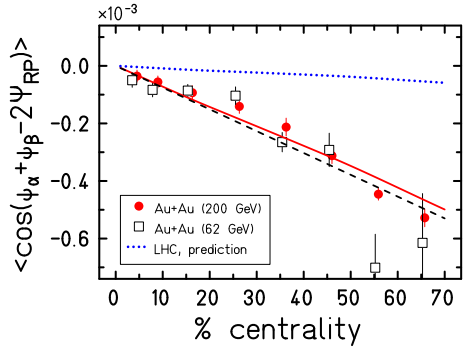

Fig. 1. Centrality dependence of the CME. Experimental points for Au+Au collisions are from [7]. The dotted line is our prediction for Au+Au collisions at the 5.5 TeV energy.

In the model considered, the CME at the energy 5.5 TeV is expected to be less by a factor of about 20 as compared to those at the RHIC energy [8]. Note that at the LHC energy we applied a simplified semi-analytical model [6] for magnetic field creation. Thus, our LHC estimate should be considered as an lower limit for the CME. Recent preliminary LHC PbPb data [9] show a remarkable agreement in both the magnitude and the behavior with the results reported by STAR in Au–Au collisions at $\sqrt{s_{NN}} = 200$ GeV. Preliminary kinetic calculations at the LHC energy 2.76 TeV increase the maximal magnetic field by a factor about three but it does not influence essentially on the relaxation time.

3. Kinetic consideration

The discussed CME signal, the electric charge asymmetry with respect to the reaction plane, can originate not only from the spontaneous local CP violation but also be simulated by other possible effects. In this respect it is important to consider the CME background. We shall do that considering a full evolution of nucleus–nucleus collisions in terms of the HSD transport model [11] and including formation of electromagnetic field as well as its evolution and impact on particle propagation.

Generalized on-shell transport equations for N strongly interacting particles in the presence of electromagnetic fields can be written as [14]

$$\left\{\frac{\partial}{\partial t} + \left(e\vec{E} + \left(\frac{e}{c}\right)\ \vec{v}\times\vec{B}\right)\nabla_{\vec{p}}\right\} f(\vec{r},\vec{p},t) = I_{\rm coll}(f, f_1, ...f_{N-1})\,, \qquad (6)$$

which are supplemented by the wave equation for the magnetic field whose solution in the semi-classical approximation for point-like moving charges is

reduced to the retarded Liénard–Wiechert potential [6]. The quasiparticle propagation in the electromagnetic field is calculated according to $d\vec{p}/dt = e\vec{E} + (e/c)\ \vec{v} \times \vec{B}$.

In a nuclear collision, the magnetic field will be a superposition of solenoidal fields from different moving charges. It is illustrated in Fig. 2. Its first panel is taken at a quite early compression stage with $t = 0.05\,\mathrm{fm}/c$ close to the maximal overlapping, where the magnetic field is maximal. The overlapping strongly interacting participant region has an "almond"-like shape. The nuclear region outside this almond corresponds to spectator matter which is the dominant source of the electromagnetic field at the very beginning of the nuclear collision. Note that in the HSD code the particles are subdivided into target and projectile spectators and participants not geometrically but dynamically: spectators are nucleons which suffered yet no collision. The next time moment corresponding to expansion stage is illustrated in Fig. 2 and in more detail studied in Ref. [14].

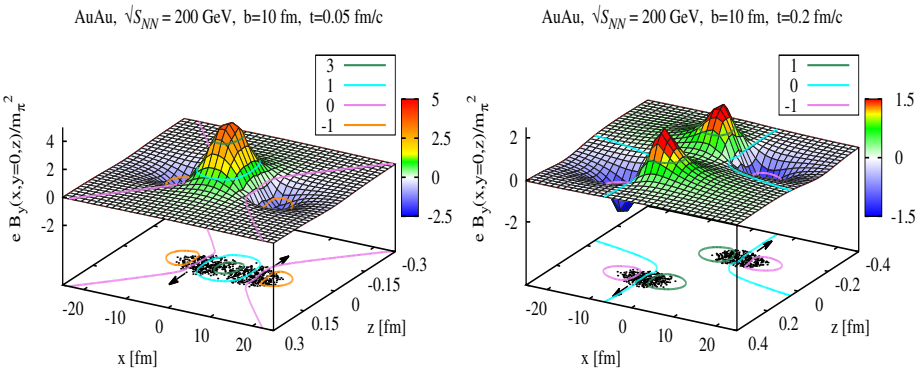

Fig. 2. Distribution of the magnetic field strength eB_y in the $y = 0$ plane at $t = 0.05$ and 0.2 fm/c for Au+Au collisions at $\sqrt{s_{NN}} = 200$ and $b = 10\,\mathrm{fm}$. The collision geometry is projected on x–z plane by points corresponding to a particular spectator position. Curves (and their projections) are levels of the constant eB_y.

The time evolution of the magnetic field and energy density at the center of the almond region $eB_y(x = 0, y = 0, z)$ for Au+Au collisions for the colliding energy $\sqrt{s_{NN}} = 200\,\mathrm{GeV}$ and the impact parameter $b = 10\,\mathrm{fm}$ is shown in Fig. 3. It is seen that the largest values of $eB_y \sim 5m_\pi^2$ are reached for a very short time. Note that this is an extremely high magnetic field, since $m_\pi^2 \approx 10^{18}$gauss. Then, the system expands and the magnetic field decreases. It is of interest to note that in our transport model, the spectator contribution to the magnetic field is practically vanishing at the center for $t \approx 1\,\mathrm{fm}/c$. In subsequent times the magnetic field eB_y is formed essentially due to produced participants with roughly equal number of negative

and positive charges which approximately compensate each other [14]. The evolution of the energy density of created particles is presented in the right panel of Fig. 3. Here, the maximal energy density (in the center of the colliding system) is $\varepsilon > 50$ GeV/fm^3 at the moment of maximal overlap of the nuclei. When the system expands, it takes a sausage-like shape and the energy density drops fast. But even at the time $t \sim 0.5\,\mathrm{fm}/c$ the local energy density is seen to be above an effective threshold of a quark-gluon phase transition $\varepsilon \gtrsim 1\,\mathrm{GeV/fm}^3$. As shown in [14] the location of the maximum energy density correlates with that for the magnetic field.

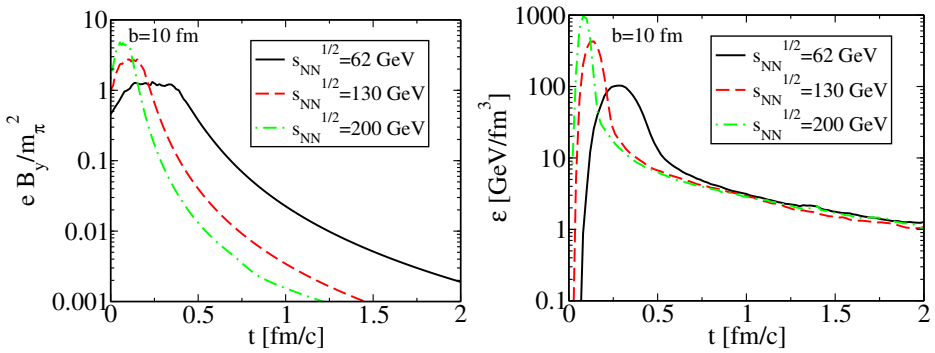

Fig. 3. Time evolution of the magnetic field strength eB_y (left) and energy density (right) at the central point $x = 0$, $y = 0$ and $z = 0\,\mathrm{fm}/c$ for Au+Au collisions at various RHIC energies.

The background electric field, being orthogonal to the magnetic one, is directed along the x axis. The evolution of the eE_x field for peripheral ($b = 10\,\mathrm{fm}$) collisions of Au+Au at the top RHIC energy is presented in Fig. 4. Similar to the case of the magnetic field, the $eE_x(x, y = 0, z)$ distribution is also inhomogeneous and closely correlates with geometry while the field strength looks "hedgehog" shaped. When the two nuclei collide, the electric fields in the overlap region significantly compensate each other, and the electric field $\vec{E}$ in the target and projectile spectator parts have opposite signs. As a result, the locations of the maximum/minimum are not in the central point of the overlap region — as they are for the magnetic field — but shifted slightly outside. The maximum of the electric field can be quite large. All these features are seen explicitly in Fig. 4, where the temporal evolutions of $eE_x(x, 0, z)$ and $eE_y(x, 0, z)$ are given. Due to destructive interference or the "hedgehog" effect, the electric field in the central part of the overlap region ($x \approx 0\,\mathrm{fm}$) is consistent with zero apart from a short period just before reaching maximal overlap. Note that the electric field at the central point is negligible for $t \gtrsim 0.15\,\mathrm{fm}/c$.

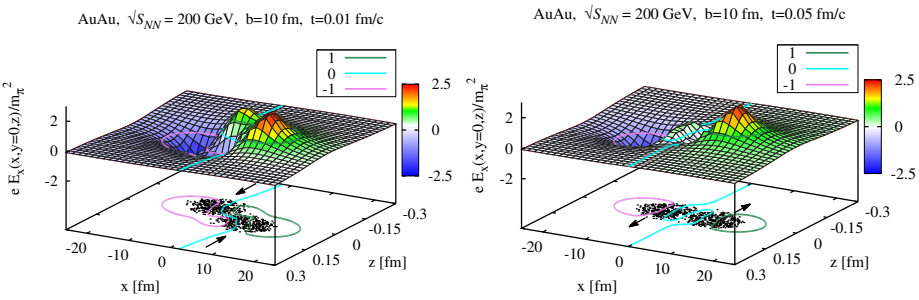

Fig. 4. (Color online) Evolution of the x- and y-components of the electric field at incoming and maximal overlap in Au+Au ($\sqrt{s} = 200\,\mathrm{GeV}$) collisions at the impact parameter $b = 10\,\mathrm{fm}$. The $eE_x = \mathrm{const.}$ levels and spectator points are shown in the projection on the (x–z) plane.

4. Observables and electric charge separation

The HSD model quite successfully describes many observables in a large range of the collision energy. Here, we investigate to what extent the electromagnetic field — incorporated in the HSD approach — will affect some observables. We shall limit ourselves to Au+Au collisions at $\sqrt{s_{NN}} = 200\,\mathrm{GeV}$ and impact parameter $b = 10\,\mathrm{fm}$. Here, we calculate the whole nuclear interaction including the decays of resonances at least up to times of $50\,\mathrm{fm}/c$.

The HSD results for the versions without and with electromagnetic field are presented in Fig. 5. With a high degree of accuracy, we see no difference between these two versions in the transverse mass m_t and rapidity y. In Fig. 6, the transverse momentum dependence of the elliptic flow of charged pions is compared for two versions (with and without field) of the HSD model. We do not observe any significant difference between the two cases.

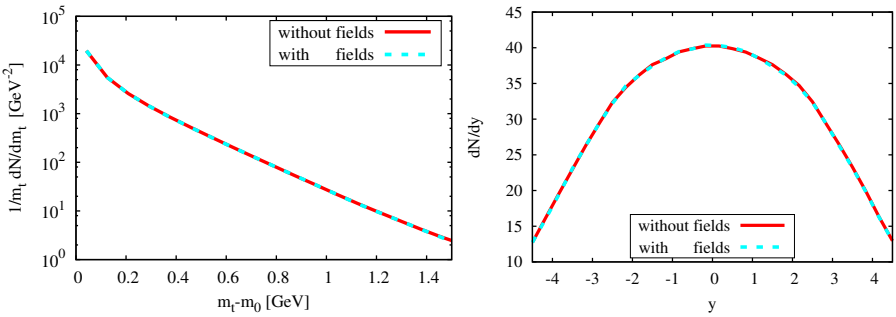

Fig. 5. Transverse mass and rapidity distributions of charged pions produced in Au+Au ($\sqrt{s_{NN}} = 200\,\mathrm{GeV}$) collisions at $b = 10\,\mathrm{fm}$. The results calculated with and without electromagnetic field are plotted by the dotted and solid lines, respectively.

Slight differences are seen in the range of $p_t \sim 1$ GeV/c but certainly it cannot be considered as significant. Note that generally the HSD model underestimates the elliptic flow, but an inclusion of partonic degrees of freedom within the PHSD approach allows to describe perfectly well the p_t dependence of v_2 at the top RHIC energy [15]. The correlator (2) is calculated on

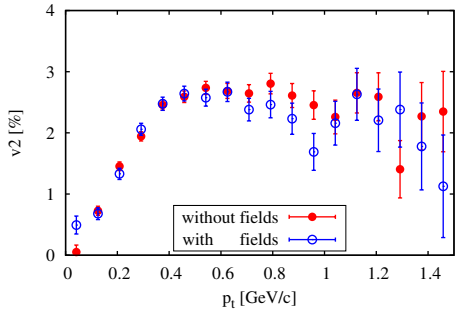

Fig. 6. The transverse momentum dependence of the elliptic flow for Au+Au ($\sqrt{s_{NN}} = 200$ GeV) collisions at $b = 10$ fm.

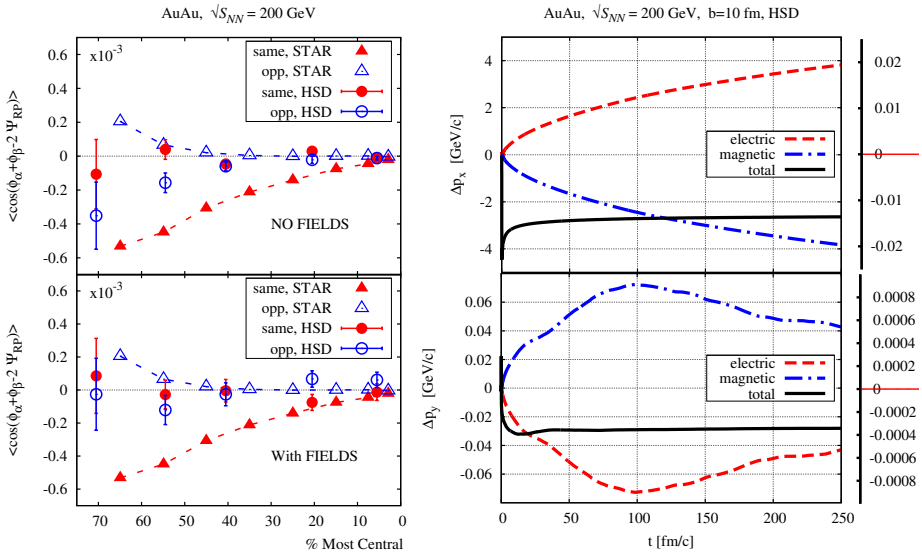

Fig. 7. Left: Azimuthal correlation in the transverse plane *vs.* centrality for like and unlike charged pions from Au+Au ($\sqrt{s_{NN}} = 200$ GeV) collisions. The experimental points — connected by lines — are taken from [7]. Right: Time dependence of the momentum increment of mesons created in Au+Au ($\sqrt{s} = 200$ GeV) collisions with the impact parameter $b = 10$ fm within HSD. Numbers along the right axis show the total transverse momentum increment Δp due to electric and magnetic fields.

the event-by-event basis. The experimental data from the STAR Collaboration [7] and the results of HSD calculations are presented in the left panel of Fig. 7. The experimental acceptance $|\eta| < 1$ and $0.15 < p_{\rm t} < 2\,{\rm GeV}$ were also incorporated in theoretical calculations. Note that the theoretical reaction plane is fixed exactly by the initial conditions and therefore is not defined by a correlation with a third charged particle as in the experiment [7]. As is seen, the HSD model shows no charge separation effect. The reason of that is explained in the right panel of Fig. 7. The average momentum increment Δp due to electric and magnetic fields is almost completely compensated in transverse component.

5. Conclusions

The model energy dependence of electric like-charge pairs can be reconciled with experiment [7] by a detailed treatment of the lifetime taking into account both the time of being in a strong magnetic field and time evolution of the energy density in the QGP phase. For the chosen parameters, we are able to describe RHIC data for Au+Au collisions on electric charge separation at two available energies. We predict that the effect will be much smaller at the LHC energy and will sharply disappear near the top energy of SPS. Coming experiments at the Large Hadron Collider [9] and that of the planned Beam Energy Scan program at RHIC [8] are of great interest since they will allow one to test the CME scenario and to infer the critical magnetic field $eB_{\rm crit}$ governing the spontaneous local CP violation.

We have extended the hadron string dynamics model for describing the formation of the retarded electromagnetic field, its evolution during a nuclear collision and the effect of this field on particle propagation. The case of the Au+Au collision at $\sqrt{s_{NN}} = 200\,{\rm GeV}$ for $b = 10\,{\rm fm}$ is considered in great detail. It is shown that the most intensive magnetic field oriented perpendicularly to the reaction plane is formed during the time when the Lorentz-contracted nuclei are passing through each other, $t \lesssim 0.2\,{\rm fm}/c$. The maximal strength of the magnetic field here attains very high values, $eB_y/m_\pi^2 \sim 5$. However, due to the compensation effect, the electromagnetic field does not influence on observables and, in particular, on the asymmetry of charged mesons with respect to the reaction plane.

We thank our collaborators E. Bratkovskaya, W. Cassing, S. Voloshin and V. Konchakovski for useful discussion and remarks. This work was supported by the LOEWE Center HIC for FAIR. V.V. is supported in part by the Russian Fund for Basic Research under grant No. 11-02-01538-a.

REFERENCES

[1] D. Kharzeev, *Phys. Lett.* **B633**, 260 (2006).

[2] D. Kharzeev, A. Zhitnitsky, *Nucl. Phys.* **A797**, 67 (2007).

[3] D.E. Kharzeev, L.D. McLerran, H.J. Warringa, *Nucl. Phys.* **A803**, 227 (2008).

[4] K. Fukushima, D.E. Kharzeev, H.J. Warringa, *Phys. Rev.* **D78**, 074033 (2008).

[5] D.E. Kharzeev, H.J. Warringa, *Phys. Rev.* **D80**, 034028 (2009).

[6] V. Skokov, A. Illarionov, V. Toneev, *Int. J. Mod. Phys.* **A24**, 5925 (2009).

[7] S. Voloshin [STAR Collaboration], *Nucl. Phys.* **A830**, 377c (2009); B.I. Abelev *et al.* [STAR Collaboration], *Phys. Rev.* **C81**, 054908 (2010); B.I. Abelev *et al.* [STAR Collaboration], *Phys. Rev. Lett.* **103**, 251601 (2009).

[8] D. Gangadharan [STAR Collaboration], *J. Phys. G: Nucl. Part. Phys.* **38**, 124166 (2011).

[9] P. Christakoglou [ALICE Collaboration], *J. Phys. G: Nucl. Part. Phys.* **38**, 124165 (2011).

[10] V. Toneev, V. Voronyuk, `arXiv:1011.5589v1 [nucl-th]`; *Phys. Part. Nucl. Lett.* **8**, 938 (2011) [`arXiv:1012.0991v1 [nucl-th]`]; *Phys. At. Nucl.* **75**, 650 (2012) [`arXiv:1012.1508v1 [nucl-th]`].

[11] W. Cassing, E.L. Bratkovskaya, *Phys. Rep.* **308**, 65 (1999).

[12] S.A Voloshin, *Phys. Rev.* **C70**, 057901 (2004).

[13] D. Kharzeev, M. Nardi, *Phys. Lett.* **B507**, 121 (2001).

[14] V. Voronyuk, E.L. Bratkovskaya *et al.*, *Phys. Rev.* **C83**, 054911 (2011).

[15] W. Cassing, E.L. Bratkovskaya, *Phys. Rev.* **C78**, 034919 (2008).